Resurgence flows in three-dimensional periodic porous media

Pierre M. Adler*
Sisyphe, Université P.-M. Curie Paris VI, Tour 46, Place Jussieu, 75252 Paris Cedex 05, France

Vladimir V. Mityushev
Department of Mathematics, Pedagogical University, ul. Podchorazych 2, Krakow 30-084, Poland
(Received 13 May 2010; published 29 July 2010)

Three-dimensional flows are addressed in porous media with resurgences. These media are characterized by a double structure, i.e., a continuous porous medium and capillaries with impermeable walls which relate distant points of the continuous medium. Spatially periodic harmonic functions with singularities at given points are constructed by means of the Berdichevskij functions; these functions extend to three dimensions the classical Weierstrass functions. The solution of the same medium with two vertices is obtained in two and three dimensions and thoroughly compared and discussed.

DOI: 10.1103/PhysRevE.82.016317 PACS number(s): 47.56.+r, 47.63.mf, 91.60.Np

I. INTRODUCTION

On the large scale, porous media are usually described by the Darcy equation with a permeability which depends on space in the case of heterogeneous materials. In most situations, these media contain fractures which may be addressed either by the classical double porosity model [1] or by the detailed approach of [2].

More recently, Ref. [3] addressed the problem of resurgence in reservoirs which occurs when a portion of an underground domain is connected to a distant one while it is not connected to closer portions. Such a phenomenon can only be understood if there exists a direct link between the two portions and if this link has little if any interaction with the porous medium that it crosses.

This phenomenon was called resurgence because of its obvious analogy with rivers which disappear from the ground surface and reappear further away. Similar ideas have already been developed in two other fields. In physics, random networks limited to nearest neighbors have been recently extended to small world models where distant vertices are related directly by a link [4]. The electrical testing of porous media by electrical probes located at the walls is a noninvasive technique called electrical tomography which has been used frequently in geophysics; a series of electrodes are placed on a wall; two of them are used to inject the current and the resulting potential differences are measured at the others (see [5] for a recent application). The distribution of the resistivities inside the material can be derived by inverting the measurements which requires the resolution of the Laplace equation. The present contribution provides a framework where the electrodes could be located on one or several surfaces bounding the analyzed medium and also inside the medium.

There are other situations which could be analyzed by means of the resurgence concept and they belong to the domain of solid mechanics. Reticulated structures made of beams of various shapes are often used in practice and the theory of these structures has been developed in the framework of homogenization theory by [6,7]. The present theory could be used with adequate changes to mixed media composed of reticulated structures interacting with three-dimensional solids.

The governing equations for flow through porous media with resurgences were detailed in [3]. Basically, the media are viewed as the superposition of a continuum medium where flow is described by Darcy law and of a capillary network where flow obeys Kirchhoff laws. Solutions were proposed for one- and two-dimensional (2D) flows. Applications to other physical phenomena were also discussed.

The major objective of this paper is to derive solutions in three dimensions when the medium is spatially periodic and when the sizes of the connections between the continuous medium and the capillary network are small with respect to the other length scales which characterize the material. The derivation of these solutions requires advanced mathematical techniques.

This paper is organized as follows. In Sec. II, the governing equations for the continuous medium and the capillary network are recalled from [3] and a general expression for the macroscopic total permeability is given.

Section III provides a detailed solution to these equations when the injection domains which relate the continuous medium and the capillary network are small with respect to the other characteristic dimensions. This necessitates the use of the triply periodic Berdichevskij (Berdichevsky) functions [8] which replace the classical Weierstrass functions employed in the two-dimensional solutions derived in [3].

Section IV details the application of the general solution to a medium with two injection domains whose positions are varied. Very different flow configurations can be obtained. Moreover, the same configurations are addressed in two and three dimensions which yield interesting comparisons between the solutions. Section V concludes this paper and proposes some extensions which are currently under study.

II. GENERAL

The dimensionless general equations which govern resurgence flows in porous media are only summarized in this

*pierre.adler@upmc.fr

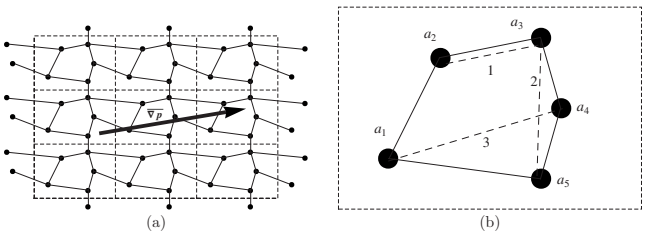

FIG. 1. Medium composed of a capillary network and of a continuous medium. (a) For simplicity, a two-dimensional picture of the whole graph is presented. (b) The local graph corresponding to the periodic graph in (a).

section since an extended presentation can be found in [3]. The medium is assumed to be composed of a capillary network and of a continuous medium which are connected at some vertices of the network as it is schematized in Fig. 1(a).

The medium is spatially periodic with a unit cell $\mathcal{Q}_0$ which is assumed to be an orthogonal parallelepipedon; hence, the fundamental translation vectors can be written as

$$\mathbf{i}_1 = (\ell_1,0,0), \quad \mathbf{i}_2 = (0,\ell_2,0), \quad \mathbf{i}_3 = (0,0,\ell_3). \tag{2.1}$$

Then, the volume of $\mathcal{Q}_0$ is equal to

$$\tau = \ell_1\ell_2\ell_3. \tag{2.2}$$

The whole medium can be generated by translations whose general form is

$$\mathbf{R_m} = m_1\mathbf{i}_1 + m_2\mathbf{i}_2 + m_3\mathbf{i}_3, \tag{2.3}$$

where $\mathbf{i}_l$ $(l=1,2,3)$ are the fundamental translation vectors; $\mathbf{m}$ is equal to (m_1,m_2,m_3), where m_l is an integer. Let $\mathbf{x}=(x_1,x_2,x_3)$ be a point in $\mathbb{R}^3$.

The network can be treated as a spatially periodic graph. It is composed of N vertices located at $\mathbf{a}_n=(a_{1n},a_{2n},a_{3n})$ $(n=1,2,\ldots,N)$ and M edges which join vertices. This graph can be presented as a finite graph with vertices at $\mathbf{a}_n$ $(n=1,2,\ldots,N)$ on the three-dimensional torus derived from the unit cell $\mathcal{Q}_0$ by identifying the opposite faces of $\mathcal{Q}_0$. Such graphs are called the local graphs [see Fig. 1(b)]. Let $V\Gamma=\{\mathbf{a}_n, n=1,2,\ldots,N\}$ and $E\Gamma=\{e_k, k=1,2,\ldots,M\}$ denote the sets of vertices and of edges of Γ. The vertices $\mathbf{a}_n+\mathbf{R_m}$ are said to be homologous to $\mathbf{a}_n \in V\Gamma$. Choose an arbitrary orientation for the edges, and define a scalar flow rate J_k along the vector,

$$\mathbf{R}(k) = (R_{k1},R_{k2},R_{k3}), \tag{2.4}$$

corresponding to the edge e_k.

A pressure may be assigned to each vertex of the network, say $p_n(\mathbf{a}_n+\mathbf{R_m})$, where $\mathbf{R_m}$ is given by Eq. (2.3). Let the external pressure gradient ∇p be applied to the medium. The periodicity of the local pressure gradient permits the local pressure to be decomposed into the sum

$$p_n(\mathbf{a}_n + \mathbf{R_m}) = p_n + \mathbf{R_m}\cdot\overline{\nabla p}, \tag{2.5}$$

where for shortness p_n denotes the pressure at $\mathbf{a}_n$.

According to [3], the flow rate J_k between two adjacent vertices through the capillary k is assumed to be proportional to the pressure drop between these vertices,

$$J_k = \alpha_k[p_{n'}(\mathbf{a}_{n'} + \mathbf{R_{m'}}) - p_n(\mathbf{a}_n + \mathbf{R_m})], \tag{2.6}$$

where the edge e_k joins the vertex $\mathbf{a}_{n'}$ to the vertex $\mathbf{a}_n$. α_k $(k=1,\ldots,M)$ are positive constants.

To each vertex $\mathbf{a}_n$ corresponds a domain D_n homeomorphic to balls with smooth surfaces ∂D_n oriented in such a way that the normal vector is directed out of D_n. These domains are supposed not to overlap. Let D be the complementary of the unit cell $\mathcal{Q}_0$ to all domains D_n.

The flow in the spatially periodic porous medium D is governed by the Darcy law and the Darcy equation,

$$\mathbf{v} = -\mathbf{K}\cdot\nabla p, \quad \nabla\cdot(\mathbf{K}\cdot\nabla p) = 0, \tag{2.7}$$

where $\mathbf{v}$ denotes the local seepage velocity, $\mathbf{K}$ is the permeability tensor, and ∇p is the local pressure gradient. The pressure gradient is spatially periodic and the pressure field verifies

$$p(\mathbf{x}+\mathbf{R_m}) = p(\mathbf{x}) + \mathbf{R_m}\cdot\overline{\nabla p} \tag{2.8}$$

where $p(\mathbf{x})$ is spatially periodic.

In order to match the continuum with the network, consider a capillary as a capillary E_k connecting two domains D_n and $D_{n'}$. The distance between D_n and $D_{n'}$ is denoted by L_k and an order of magnitude of the width of E_k by d_k. These two quantities are assumed to verify

$$d_k \ll L_k. \tag{2.9}$$

In other words, the two injection domains should not be too close in order to be considered as punctual with a good approximation in the continuum domain. The corresponding error in the estimation of the macroscopic properties is expected to be of the order $(d_k/L_k)^2$ as in the classical Clausius-Mossoti equation [11].

Two boundary conditions are applied at the vertices which connect the network and the continuous porous medium, or more precisely at the surfaces ∂D_n. First, the pressure p is assumed to be constant and equal to p_n at ∂D_n. Therefore,

$$p(\mathbf{x}) = p_n, \quad \mathbf{x} \in \partial D_n, \quad n = 1,2,\ldots,N. \tag{2.10}$$

Second, the flow rates j_n from the capillaries into the continuum must verify

$$\sum_{k\in\Omega(n)} \alpha_k[p_n - p_{n'}(\mathbf{a}_{n'} + \mathbf{R_{m'}})] = \int_{\partial D_n} d\mathbf{s}\cdot\mathbf{K}\cdot\nabla p = -j_n,$$

$$n = 1,2,\ldots,N, \tag{2.11}$$

where $p_{n'}(\mathbf{a}_{n'}+\mathbf{R_{m'}})$ is expressed in terms of $p_{n'}$ by Eq. (2.5).

Thus, the following boundary value problem is obtained. The field $p(\mathbf{x})$ obeys Eq. (2.7) in D and is continuously differentiable in the closure of D; it satisfies the quasiperiodic relations (2.8) and the boundary conditions (2.10) and (2.11). The constants p_n $(n=1,2,\ldots,N)$ have to be determined after this problem is solved.

The problem is well stated and it is nonlocal. When $\mathbf{K}$ is supposed to be isotropic and constant in D, $\mathbf{K}(\mathbf{x})=K\mathbf{I}$ and Eq. (2.7) is reduced to the Laplace equation

$$\nabla^2 p = 0. \tag{2.12}$$

In this case, Eq. (2.11) can be simplified as

$$\sum_{k\in\Omega(n)} \alpha_k [p_n - p_{n'}(\mathbf{a}_{n'} + \mathbf{R}_{\mathbf{m}'})] = K \int_{\partial D_n} \frac{\partial p}{\partial \mathbf{n}} ds = -j_n,$$

$$n = 1,2,\ldots,N. \tag{2.13}$$

Note that the flow rates j_n verify [3]

$$\sum_{n=1}^{N} j_n = 0. \tag{2.14}$$

Finally, the most important quantity is the permeability $\bar{\mathbf{K}}$ which can be derived from the average total velocity in the medium which is defined as the integral over the continuous medium plus the integral over the capillaries [3] in the cell $\mathcal{Q}_o$,

$$\bar{\mathbf{v}} = \frac{1}{\tau}\left[\int_D \mathbf{v} d^3\mathbf{x} + \int_V \mathbf{v} d^3\mathbf{x}\right] = -\bar{\mathbf{K}} \cdot \overline{\boldsymbol{\nabla} p}. \tag{2.15}$$

In order to derive a compact expression for $\bar{\mathbf{K}}$, it is usual [10] to introduce higher-order vectors and tensors by

$$p(\mathbf{x}) = \mathcal{P}(\mathbf{x}) \cdot \overline{\boldsymbol{\nabla} p}, \quad J_k = \mathcal{J}_k \cdot \overline{\boldsymbol{\nabla} p}, \quad \mathbf{v}(\mathbf{x}) = \mathcal{V}(\mathbf{x}) \cdot \overline{\boldsymbol{\nabla} p}, \tag{2.16}$$

where $\mathcal{P}(\mathbf{x})$ and $\mathcal{J}_k$ are vectors while $\mathcal{V}(\mathbf{x})$ is a second-order tensor. Then, it is an easy matter to introduce these definitions into Eq. (2.15) and to obtain

$$\bar{\mathbf{K}} = -\frac{1}{\tau}\left[\int_{\partial \mathcal{Q}_0} \mathbf{x} ds\, \mathbf{n} \cdot \mathcal{V} + \sum_{k=1}^{M} \mathbf{R}(k) \mathcal{J}_k\right]. \tag{2.17}$$

The vectors $\mathcal{P}(\mathbf{x})$ and the tensor $\mathcal{V}(\mathbf{x})$ can be determined by three flows produced by three linearly independent pressure gradients parallel to the three axes,

$$\overline{\boldsymbol{\nabla} p}^{(1)} = (1,0,0)^\dagger, \quad \overline{\boldsymbol{\nabla} p}^{(2)} = (0,1,0)^\dagger, \quad \overline{\boldsymbol{\nabla} p}^{(3)} = (0,0,1)^\dagger, \tag{2.18}$$

where $\mathbf{X}^\dagger$ stands for the transposed vector $\mathbf{X}$.

In the following, the macroscopic pressure gradient will be oriented most of the time along the x_1 axis. Therefore, the previous equations become

$$[p(\mathbf{x})]_1 = \ell_1, \quad [p(\mathbf{x})]_2 = [p(\mathbf{x})]_3 = 0, \tag{2.19}$$

where the brackets $[\ ]_s$ denote the jump $[f(\mathbf{x})]_s = f(\mathbf{x}+\mathbf{i}_s) - f(\mathbf{x})$ $(s=1,2,3)$. The first row of Eq. (2.17) becomes

$$\bar{\mathbf{K}}_1 = -\frac{1}{\tau}\int_{\partial \mathcal{Q}_0} \mathbf{x} ds \cdot \mathbf{v} - \frac{1}{\tau}\sum_{k=1}^{M} J_k \mathbf{R}(k). \tag{2.20}$$

III. SMALL INJECTION DOMAINS

In the present section, it is assumed that D_n are balls of a sufficiently small radius r with centers at $\mathbf{a}_n$. Then, the boundary condition (2.10) for the pressure $p(\mathbf{x})$ can be replaced with an asymptotic formula for $p(\mathbf{x})$ at $\mathbf{a}_n$ $(n=1,2,\ldots,N)$. In Sec. III A, a formula for $p(\mathbf{x})$ is constructed with the prescribed properties. Then, the result is used in Sec. III B to deduce formula (3.44) for the total permeability valid for small injection domains.

A. Local field

1. Properties of pressure

For a locally isotropic medium, the pressure $p(\mathbf{x})$ satisfies the Laplace equation (2.12) in the whole cell $\mathcal{Q}_0$ except the points $\mathbf{a}_n$ $(n=1,2,\ldots,N)$ where it has a singularity corresponding to the flow injection from the capillaries. Hence, the local behavior of $p(\mathbf{x})$ near $\mathbf{a}_n$ is described by the asymptotic formula

$$p(\mathbf{x}) \sim \frac{j_n}{4\pi K}\frac{1}{|\mathbf{x}-\mathbf{a}_n|} + p_n^{(0)}, \quad \text{as } \mathbf{x} \to \mathbf{a}_n, \quad n = 1,2,\ldots,N, \tag{3.1}$$

where j_n is related to the flow rates in the network by Eq. (2.11); $p_n^{(0)}$ are constants. Moreover, the gradient $\boldsymbol{\nabla} p(\mathbf{x})$ is triply periodic and $p(\mathbf{x})$ has given jumps per cell along the three axes. Therefore, the quasiperiodicity conditions (2.19) are taken into account. The pressure $p(\mathbf{x})$ is constructed in Sec. III A 2 in terms of the triply periodic Berdichevskij's functions which are summarized in the next section.

2. Berdichevskij functions

The basic function in this construction is a function $\wp(\mathbf{x})$ harmonic in $\mathcal{Q}_0$ except at the origin with the asymptotic behavior

$$\wp(\mathbf{x}) \sim |\mathbf{x}|^{-1}, \quad \text{as } \mathbf{x} \to \mathbf{0}. \tag{3.2}$$

Such a spatially periodic function does not exist. However, it is possible to construct a function which is "almost" periodic. Such a function $\wp(\mathbf{x})$ is the extension to three dimensions of the two-dimensional Weierstrass function $\ln \sigma(z)$ described and used in [3].

Consider the centers of the cells $\mathbf{R}_\mathbf{m}$ introduced by Eq. (2.3). The desired function $\wp(\mathbf{x})$ cannot be directly defined by the divergent series $\Sigma_\mathbf{m}|\mathbf{x}-\mathbf{R}_\mathbf{m}|^{-1}$. Similarly to elliptic functions, $\wp(\mathbf{x})$ can be introduced by integration of absolutely convergent series.

Berdichevskij [8] introduced nine functions $\wp_{ij}(\mathbf{x})$ in such a way that they are spatially periodic and have the prescribed singularities at zero, i.e.,

$$\wp_{ij}(\mathbf{x}+\mathbf{i}_1) = \wp_{ij}(\mathbf{x}+\mathbf{i}_2) = \wp_{ij}(\mathbf{x}+\mathbf{i}_3) = \wp_{ij}(\mathbf{x}), \tag{3.3a}$$

$$\wp_{ij}(\mathbf{x}) \sim \frac{\partial^2}{\partial x_i\, \partial x_j}\left(\frac{1}{|\mathbf{x}|}\right), \quad \text{as } \mathbf{x} \to \mathbf{0} \quad (i,j=1,2,3). \tag{3.3b}$$

Each function $\wp_{ij}(\mathbf{x})$ can be written as

$$\wp_{ij}(\mathbf{x}) = \frac{\partial^2}{\partial x_i\,\partial x_j}\left(\frac{1}{|\mathbf{x}|}\right) + \sum_{\mathbf{m}\in\mathbb{Z}^3\backslash\mathbf{0}}\left[\frac{\partial^2}{\partial x_i\,\partial x_j}\left(\frac{1}{|\mathbf{x}-\mathbf{R_m}|}\right) - \frac{\partial^2}{\partial x_i\,\partial x_j}\left(\frac{1}{|\mathbf{x}-\mathbf{R_m}|}\right)\Bigg|_{\mathbf{x}=\mathbf{0}}\right], \tag{3.4}$$

where $\mathbb{Z}^3\backslash\mathbf{0}$ denotes the set of triple integers $\mathbf{m}=(m_1,m_2,m_3)$ except the origin zero. The series (3.4) are absolutely convergent as series equivalent to the absolutely convergent series $\Sigma_{\mathbf{m}}|\mathbf{x}-\mathbf{R_m}|^{-4}$ in D. The periodic functions $\wp_{ij}(\mathbf{x})$ $(i,j=1,2,3)$ correspond to the real and imaginary parts of the classical two-dimensional $\wp$ function of Weierstrass. The desired function $\wp(\mathbf{x})$ is obtained by the double integration of $\wp_{ij}(\mathbf{x})$ to get the asymptotic behavior (3.2). This integration applied to Eq. (3.3) yields quasiperiodicity conditions for $\wp(\mathbf{x})$. It is worth noting that Eq. (3.4) cannot be integrated term by term since divergent series arise.

Let L be a curve connecting the points 0 and $\mathbf{x}$ which does not contain any point $\mathbf{R_m}$. Introduce the functions

$$\wp_i(\mathbf{x}) = \frac{\partial}{\partial x_i}\left(\frac{1}{|\mathbf{x}|}\right) + \int_L \sum_{j=1,2,3}\left[\wp_{ij}(\mathbf{y}) - \frac{\partial^2}{\partial y_i\,\partial y_j}\left(\frac{1}{|\mathbf{y}|}\right)\right]dy_j \quad (i=1,2,3), \tag{3.5}$$

where $\mathbf{y}=(y_1,y_2,y_3)$. The desired function $\wp(\mathbf{x})$ is given by the integral

$$\wp(\mathbf{x}) = \frac{1}{|\mathbf{x}|} + \sum_{i=1,2,3}\int_L\left[\wp_i(\mathbf{y}) - \frac{\partial}{\partial y_i}\left(\frac{1}{|\mathbf{y}|}\right)\right]dy_i. \tag{3.6}$$

The use of Eqs. (3.4) and (3.5) and integration of Eq. (3.6) imply that $\wp(\mathbf{x})$ can be written as an absolutely convergent series,

$$\wp(\mathbf{x}) = \frac{1}{|\mathbf{x}|} + \sum_{\mathbf{m}\in\mathbb{Z}^3\backslash\mathbf{0}}\left[\frac{1}{|\mathbf{x}-\mathbf{R_m}|} - \frac{1}{|\mathbf{R_m}|} - \frac{\mathbf{R_m}\cdot\mathbf{x}}{|\mathbf{R_m}|^3} - \frac{6(\mathbf{R_m}\cdot\mathbf{x})^2}{|\mathbf{R_m}|^5} + \frac{|\mathbf{x}|^2}{2|\mathbf{R_m}|^3}\right]. \tag{3.7}$$

Therefore, the nine periodic functions $\wp_{ij}(\mathbf{x})$ defined by Eq. (3.4), the three functions $\wp_i(\mathbf{x})$ defined by Eq. (3.5), and one quasiperiodic function $\wp(\mathbf{x})$ represented as the series (3.7) have been constructed.

According to [8], $\wp(\mathbf{x})$ is an even function harmonic in $\mathcal{Q}_0\backslash\{\mathbf{0}\}$ and its jumps per cell coincide with the jumps of the quadratic function

$$d(\mathbf{x}) = \frac{1}{2}\mathbf{x}\cdot\boldsymbol{\gamma}\cdot\mathbf{x}^{\dagger}. \tag{3.8}$$

The tensor $\boldsymbol{\gamma}$ is introduced through the jumps of $\wp_i(\mathbf{x})$ per cell,

$$\gamma_{ij} = [\wp_i(\mathbf{x})]_j\ell_j. \tag{3.9}$$

For the cubic cell $(\ell_1=\ell_2=\ell_3=\ell)$, Eq. (3.9) becomes

$$\gamma_{ij} = -\frac{4\pi}{3\ell^3}\delta_{ij}, \tag{3.10}$$

where δ_{kj} is the Kronecker symbol.

Expand the function $\wp(\mathbf{x})$ into the series

$$\wp(\mathbf{x}) = \frac{1}{|\mathbf{x}|} + \frac{1}{4!}\sum_{i,j,k,l}\wp'_{ijkl}(\mathbf{0})x_ix_jx_kx_l + \frac{1}{6!}\sum_{i,j,k,l,m,n}\wp'_{ijklmn}(\mathbf{0})x_ix_jx_kx_lx_mx_n + \cdots, \tag{3.11}$$

where the summation indices run over 1,2,3. Here, it is taken into account that the regular part of $\wp(\mathbf{x})$ begins at least from the third-order terms and that $\wp(\mathbf{x})$ is an even function. The constants $\wp'_{ijkl}(\mathbf{0})$ and $\wp'_{ijklmn}(\mathbf{0})$ can be easily calculated for some symmetric lattices. The invariance of $\wp(\mathbf{x})$ with respect to a symmetry group implies that the coefficients of $\wp(\mathbf{x})$ are also invariant. The general theory of tensors [8] implies that isotropic and homogeneous tensors of order 4 and higher must have special structures. In particular,

$$\wp'_{ijkl}(\mathbf{0}) = t_1\left(\frac{4\pi}{3\ell^3}\right)^{5/3}\left[o_{ijkl} - \frac{1}{5}(\delta_{ij}\delta_{kl} + \delta_{ik}\delta_{jl} + \delta_{il}\delta_{jk})\right], \tag{3.12}$$

$$\wp'_{ijklmn}(\mathbf{0}) = t_2\left(\frac{4\pi}{3\ell^3}\right)^{7/3}\left[\frac{77}{2}\sum_{s=1,2,3}o_{ijks}o_{slmn} - \frac{7}{2}(\delta_{(ij}o_{klmn)} + \delta_{(ij}\delta_{kl}\delta_{mn)})\right], \tag{3.13}$$

where $t_{1,2}$ are constants; the tensor o_{ijkl} has only three nontrivial components $o_{iiii}=1$ $(i=1,2,3)$. The brackets in the subscripts denote the symmetrization, i.e., $\delta_{(ij}o_{klmn)}$ is the sum of $\delta_{ij}o_{klmn}$ with all permutations by the subscripts i,j,k,l,m,n. For a cubic cell, $t_1=17.132\,38$ and $t_2=37.978\,46$ [8].

The properties of $\wp(\mathbf{x})$ are summarized below. The function $\wp(\mathbf{x})$ has a singularity at $\mathbf{x}=\mathbf{0}$ described by expansion (3.11). It is not spatially periodic. Their jumps per cell coincide with the jumps of the quadratic function (3.8). For the cubic lattice, the jumps of $\wp(\mathbf{x})$ can be easily estimated by Eqs. (3.11)–(3.13) as well as the jumps of $\wp(\mathbf{x}-\mathbf{a}_n)$ needed below.

The pressure can be expressed in terms of the Berdichevskij function

$$p(\mathbf{x}) = \sum_{n=1}^{N}\frac{j_n}{4\pi K}\wp(\mathbf{x}-\mathbf{a}_n) + \mathbf{b}\cdot\mathbf{x} + p_0, \tag{3.14}$$

where $\mathbf{b}$ is an undetermined constant vector. Then, the pressure $p(\mathbf{x})$ satisfies Eq. (3.1) when $\mathbf{x}$ tends toward $\mathbf{a}_n$. Below the vector $\mathbf{b}$ is chosen in such a way that conditions (2.19) hold.

Calculate the jump

$$[\wp(\mathbf{x}-\mathbf{a}_n)]_i = [d(\mathbf{x}-\mathbf{a}_n)]_i = \frac{1}{2}\gamma_{ii}\ell_i^2 + \ell_i\sum_{k=1,2,3}\gamma_{ik}(x_k-a_{kn}), \tag{3.15}$$

where $\mathbf{a}_n=\Sigma_{k=1,2,3}\mathbf{i}_ka_{kn}$. Then, Eqs. (3.14) and (2.14) imply

$$[p(\mathbf{x})]_i = -\frac{\ell_i}{4\pi K}\sum_{n=1}^{N}\sum_{k=1,2,3}\gamma_{ik}a_{kn}j_n + [\mathbf{b}\cdot\mathbf{x}]_i. \quad (3.16)$$

Relations (2.19) yield

$$\mathbf{b} = \frac{\mathbf{i}_1}{\ell_1} + \frac{1}{4\pi K}\sum_{n=1}^{N}\sum_{k,l=1,2,3}\mathbf{i}_l\gamma_{lk}a_{kn}j_n. \quad (3.17)$$

The use of Eq. (3.10) for the cubic cell ($\ell_1=\ell_2=\ell_3=\ell$) implies

$$\mathbf{b} = \frac{\mathbf{i}_1}{\ell} - \frac{1}{3\ell^3 K}\sum_{n=1}^{N}\mathbf{a}_n j_n. \quad (3.18)$$

Therefore, Eqs. (3.14) and (3.17) determine $p(\mathbf{x})$ up to an arbitrary additive constant p_0. These formulas can be used to estimate $p(\mathbf{x})$ on the spheres ∂D_n,

$$p(\mathbf{a}_n+\mathbf{r}) = \sum_{k=1}^{N}\frac{j_k}{4\pi K}\wp(\mathbf{a}_n-\mathbf{a}_k+\mathbf{r}) + \mathbf{b}\cdot(\mathbf{a}_n+\mathbf{r}) + p_0. \quad (3.19)$$

When the terms of order $O(r)$ are neglected, Eq. (3.19) implies that the pressure near ∂D_n is estimated up to $O(r)$ by the constant

$$p_n = \frac{j_n}{4\pi r K} + \sum_{k=1;\ k\neq n}^{N}\frac{j_k}{4\pi K}\wp(\mathbf{a}_n-\mathbf{a}_k) + \mathbf{b}\cdot\mathbf{a}_n + p_0. \quad (3.20)$$

These are the missing equations which complete the equations from Sec. II to determine p_n, J_k, and j_n.

3. Solutions for pressure and flow fields

Following [3,9], an algorithm is now described to calculate the required values p_n, j_n, and J_k. These values determine the flow in the network, the pressure Eq. (3.14) in the continuous problem, and the macroscopic permeability (2.20) [see also Eq. (3.44) below]. Consider any spanning tree T of the local graph Γ whose chords are labeled as $e_1, e_2, \ldots, e_{N-1}$. Introduce the vector $\mathbf{P}=(P_1,\ldots,P_M)$ whose components are the pressure differences along each edge e_k,

$$P_k = p_{n'} - p_n, \quad k = 1,2,\ldots,M. \quad (3.21)$$

If an edge e_k connects two vertices from different unit cells, formula (2.5) is used to express all P_k through the pressures p_n ($n=1,2,\ldots,N$) prescribed to the vertices from the zeroth cell $\mathcal{Q}_0$. Kirchhoff's potential law states that the pressure difference vanishes along every cycle of the graph. This law may be expressed as [see Eq. (4.28) from [9]]

$$\xi_Q\cdot\mathbf{P} = \mathbf{0}, \quad (3.22)$$

where ξ_Q runs over cycles of the graph Γ. A scalar form of Eq. (3.22) yields $M-N-1$ linearly independent equations between the components of the vector $\mathbf{P}$ with the coefficients C_{km} equal to -1, 0, or 1,

$$P_k = \sum_{m=1}^{N-1} C_{km}P_m, \quad k = N, N+1, \ldots, M. \quad (3.23)$$

Details are given in [9,10]. In accordance with Eq. (2.6),

$$J_k = \alpha_k P_k, \quad k = 1,2,\ldots,M. \quad (3.24)$$

j_n is linearly related to J_k by the $N-1$ first relations (2.13) and by Eq. (2.14) written as

$$j_n = \sum_{k\in\Omega^+(n)} J_k - \sum_{k\in\Omega^-(n)} J_k, \quad n = 1,2,\ldots,N-1, \quad (3.25a)$$

$$j_N = -\sum_{n=1}^{N-1} j_n. \quad (3.25b)$$

The components of the vector $\mathbf{P}$ can be derived from Eq. (3.20),

$$P_k = \frac{j_{n'}-j_n}{4\pi r} + \sum_{k'=1;\ k'\neq n'}^{N}\frac{j_{k'}}{4\pi}\wp(\mathbf{a}_n-\mathbf{a}_{k'}) - \sum_{k=1;\ k\neq n}^{N}\frac{j_k}{4\pi}\wp(\mathbf{a}_n-\mathbf{a}_k) + \mathbf{b}\cdot(\mathbf{a}_{n'}-\mathbf{a}_n),$$
$$n = 1,2,\ldots,N-1. \quad (3.26)$$

Equations (3.25b) and (3.26) imply

$$P_k = \sum_{k=1}^{N-1} A_{km}j_m + a_{1n'} - a_{1n}, \quad k = 1,2,\ldots,N-1, \quad (3.27)$$

where a_{1n} is the x_1 coordinate of the vertex $\mathbf{a}_n$; A_{km} is determined by the right-hand part of Eq. (3.26) and it can be explicitly written as follows. Let k be fixed; the edge e_k connects the vertices $\mathbf{a}_n$ and $\mathbf{a}_{n'}$. Then, Eqs. (3.27) and (3.18) yield

$$A_{kn} = \frac{1}{4\pi K}\left[-\frac{1}{r} + \wp(\mathbf{a}_{n'}-\mathbf{a}_n)\right] - \frac{1}{3\ell^3 K}\mathbf{a}_n\cdot(\mathbf{a}_{n'}-\mathbf{a}_n), \quad (3.28a)$$

$$A_{kn'} = \frac{1}{4\pi K}\left[\frac{1}{r} - \wp(\mathbf{a}_n-\mathbf{a}_{n'})\right] - \frac{1}{3\ell^3 K}\mathbf{a}_{n'}\cdot(\mathbf{a}_{n'}-\mathbf{a}_n), \quad (3.28b)$$

$$A_{ks} = \frac{1}{4\pi K}[\wp(\mathbf{a}_{n'}-\mathbf{a}_s) - \wp(\mathbf{a}_n-\mathbf{a}_s)] - \frac{1}{3\ell^3 K}\mathbf{a}_s\cdot(\mathbf{a}_{n'}-\mathbf{a}_n), \quad s\neq n,n'. \quad (3.28c)$$

The linear relations (3.23), (3.24), and (3.27) constitute a linear algebraic system of $2M+N-1$ equations for the $2M+N-1$ unknowns P_k, j_n, and J_k ($n=1,2,\ldots,N-1$, $k=1,2,\ldots,M$). This system always has a unique solution [3]. Then, the pressure $p(\mathbf{x})$ is derived from Eq. (3.14).

B. Macroscopic permeability

There are two ways to evaluate the macroscopic permeability $\bar{\mathbf{K}}$ or equivalently $\overline{\mathbf{K}_1}$ from Eq. (2.20). In the present section, the permeability of the continuum porous medium is assumed for simplicity to be isotropic and constant, i.e., $\mathbf{K}=K\mathbf{I}$ with $K=$const. It follows from Eq. (3.14) that

$$\boldsymbol{\nabla} p(\mathbf{x}) = \sum_{n=1}^{N} \frac{j_n}{4\pi} \sum_{m=1,2,3} \wp_m(\mathbf{x}-\mathbf{a}_n)\frac{\mathbf{i}_m}{\ell_m} + \mathbf{b}, \tag{3.29}$$

since $\wp_m=\partial\wp/\partial x_m$. Substitution of Eq. (3.29) into $\mathbf{v}=-K\boldsymbol{\nabla} p$ yields

$$\mathbf{v}(\mathbf{x}) = -K\left(\sum_{n=1}^{N} \frac{j_n}{4\pi} \sum_{m=1,2,3} \wp_m(\mathbf{x}-\mathbf{a}_n)\frac{\mathbf{i}_m}{\ell_m} + \mathbf{b}\right). \tag{3.30}$$

Then, Eq. (2.20) becomes

$$\overline{\mathbf{K}_1} = K(\mathbf{S}+\mathbf{b}) - \frac{1}{\tau}\sum_{k=1}^{M} J_k \mathbf{R}(k), \tag{3.31}$$

where the vector $\mathbf{S}$ is given by

$$\mathbf{S} = \frac{1}{\tau}\sum_{n=1}^{N} \frac{j_n}{4\pi} \int_{\partial\mathcal{Q}_0} \mathbf{x} \sum_{m=1,2,3} d\mathbf{s}\cdot\mathbf{i}_m \frac{\wp_m(\mathbf{x}-\mathbf{a}_n)}{\ell_m}. \tag{3.32}$$

In order to calculate the integral (3.32), divide $\partial\mathcal{Q}_0$ into the six rectangles which are the faces of the unit cell

$$\partial\mathcal{Q}_0 = \cup_{k=1,2,3}(S_k^+ - S_k^-). \tag{3.33}$$

On each rectangle $S_k^{\pm}$, one has $\mathbf{x}=\pm\mathbf{i}_m/2$ and $d\mathbf{s}=\pm(\mathbf{i}_m/\ell_m)dx_{k-1}dx_{k+1}$, where the subscripts are taken modulo 3. Then, Eq. (3.32) becomes

$$\mathbf{S} = \frac{1}{\tau}\sum_{n=1}^{N} \frac{j_n}{4\pi} \sum_{m=1,2,3} \mathbf{i}_m \int_{S_m^+} \wp_m(\mathbf{x}-\mathbf{a}_n)ds. \tag{3.34}$$

The surface integrals from Eq. (3.34) can be expressed by double integrals. For instance,

$$\int_{S_1^+} \wp_1(\mathbf{x}-\mathbf{a}_n)ds = \int_{-\ell_2/2}^{\ell_2/2} dx_2 \int_{-\ell_3/2}^{\ell_3/2} \wp_1\left(\frac{\ell_1}{2}-a_{1n},x_2-a_{2n},x_3-a_{3n}\right)dx_3. \tag{3.35}$$

After calculation and substitution of $\mathbf{S}$ into Eq. (3.31), the vector $\overline{\mathbf{K}_1}$ can be calculated. For the cubic lattice, formulas (3.11)–(3.13) can be applied to simplify the calculation of the integrals.

There is another way to estimate the vector $\bar{\mathbf{K}}_1$ from Eq. (2.20). Decompose the boundary of the domain D into

$$\partial D = \partial\mathcal{Q}_0 - \cup_{n=1}^{N} \partial D_n, \tag{3.36}$$

where the orientation of ∂D_n is chosen in such a way that the normal vector to ∂D_n is directed into D. Then, the integral $\mathbf{I}_D$ is decomposed in accordance with Eq. (3.36),

$$\mathbf{I}_D = \int_{\partial D} \mathbf{x}d\mathbf{s}\cdot\mathbf{v} = \int_{\partial\mathcal{Q}_0} \mathbf{x}d\mathbf{s}\cdot\mathbf{v} - \sum_{n=1}^{N}\int_{\partial D_n} \mathbf{x}d\mathbf{s}\cdot\mathbf{v}. \tag{3.37}$$

On the other hand,

$$\mathbf{I}_D = \int_D \mathbf{v}d^3\mathbf{x} = -K\int_D \boldsymbol{\nabla} p d^3\mathbf{x} = -K\int_{\partial D} p d\mathbf{s}. \tag{3.38}$$

Application of decomposition (3.36) yields

$$\mathbf{I}_D = -K\left(\int_{\partial\mathcal{Q}_0} p d\mathbf{s} - \sum_{n=1}^{N}\int_{\partial D_n} p d\mathbf{s}\right). \tag{3.39}$$

The first integral in Eq. (3.39) is easily calculated by application of Eqs. (2.19) and (3.33),

$$\int_{\partial\mathcal{Q}_0} p d\mathbf{s} = \sum_{k=1,2,3}\left(\int_{S_k^+} - \int_{S_k^-}\right) p d\mathbf{s} = \sum_{k=1,2,3} [p]_k \frac{\mathbf{i}_k}{\ell_k}\mathrm{area}(S_k^+) = \tau\frac{\mathbf{i}_1}{\ell_1}. \tag{3.40}$$

The pressure $p(\mathbf{x})$ on ∂D_n is a constant up to $O(r)$ in accordance with Eq. (3.20). Hence, each integral $\int_{\partial D_n} p d\mathbf{s}$ from Eq. (3.39) is equal to zero up to $O(r)$ and Eq. (3.39) becomes

$$\mathbf{I}_D = -K\tau. \tag{3.41}$$

Each integral $\int_{\partial D_n} \mathbf{x}d\mathbf{s}\cdot\mathbf{v}$ from Eq. (3.37) can be estimated up to $O(r)$ as

$$\int_{\partial D_n} \mathbf{x}d\mathbf{s}\cdot\mathbf{v} = \mathbf{a}_n j_n, \tag{3.42}$$

where the definition of the flow rate (2.13) is used. Therefore, Eq. (3.37) up to $O(r)$ becomes

$$-K\tau\frac{\mathbf{i}_1}{\ell_1} = \int_{\partial\mathcal{Q}_0} \mathbf{x}d\mathbf{s}\cdot\mathbf{v} - \sum_{n=1}^{N}\mathbf{a}_n j_n. \tag{3.43}$$

Then, Eq. (2.20) can be written up to $O(r)$ as

$$\bar{\mathbf{K}}_1 = K\frac{\mathbf{i}_1}{\ell_1} - \frac{1}{\tau}\left[\sum_{n=1}^{N}\mathbf{a}_n j_n + \sum_{k=1}^{M} J_k\mathbf{R}(k)\right]. \tag{3.44}$$

An algorithm to determine j_n and J_k was detailed in Sec. VIB of [3] and sketched at the end of Sec. III A. Although [3] addresses the two-dimensional case, the algorithm in the three-dimensional case repeats Sec. VIB of [3] without any change.

IV. EXAMPLES

The major objective of this section is to illustrate the previous developments by an example which is successively solved in two and three dimensions and to compare the results.

A. Two-dimensional example

Consider the periodic square lattice in Fig. 2 with the normalized sizes $\ell_1=\ell_2=\ell=1$ and with two vertices per unit

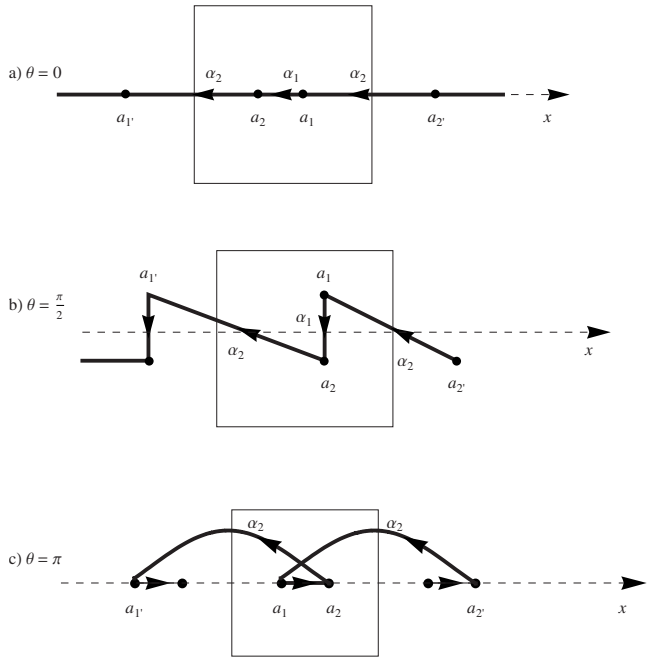

FIG. 2. The networks considered in Secs. IV A and IV B. The locations of the vertices and the angle between the vector $\mathbf{a}_1-\mathbf{a}_2$ and the x_1 axis are given by Eqs. (4.1). The unit cell is indicated by the thin solid lines.

cell $\mathbf{a}_1=(a_{11},a_{12})=\frac{1}{2}\mathbf{a}$ and $\mathbf{a}_2=(a_{21},a_{22})=-\frac{1}{2}\mathbf{a}$. Further, it is convenient to identify the vector $\mathbf{a}$ with a complex number $a=|a|e^{i\theta}$, where $|a|$ is the length of $\mathbf{a}$ and θ is the angle which $\mathbf{a}$ forms with the x_1 axis. For simplicity, the permeability is equal to 1. The vertices in the network are sequentially connected (see Fig. 2), but their locations are different. The following three cases are distinguished:

$$\mathbf{a}_1=(0.125,0),\quad \mathbf{a}_2=(-0.125,0),\quad \theta=0, \tag{4.1a}$$

$$\mathbf{a}_1=(0,0.125),\quad \mathbf{a}_2=(0,-0.125),\quad \theta=\frac{\pi}{2}, \tag{4.1b}$$

$$\mathbf{a}_1=(-0.125,0),\quad \mathbf{a}_2=(0.125,0),\quad \theta=\pi. \tag{4.1c}$$

An external gradient $\overline{\nabla p}=(1,0)$ is applied. In this example, the tree consists of one edge denoted by e_1. The very same configurations are studied in Sec. IV B in three dimensions. The three-dimensional potential $j_n/4\pi r$ in Eq. (3.20) has to be replaced with $-(j_n/2\pi)\ln r$ [3]. The function $\wp(\mathbf{x})$ is replaced with the Weierstrass function $\ln|\sigma(z)|$ [12] where the complex variable $z=x_1+ix_2$ is introduced.

According to Eq. (3.21), define

$$P_1=p_1-p_2,\quad P_2=p_2-p_{1'}. \tag{4.2}$$

Formula (3.24) becomes

$$J_1=\alpha_1 P_1,\quad J_2=\alpha_2 P_2. \tag{4.3}$$

Let $j_1=j$; then, $j_2=-j$ in accordance with Eq. (3.25b). Equations (3.25a) become

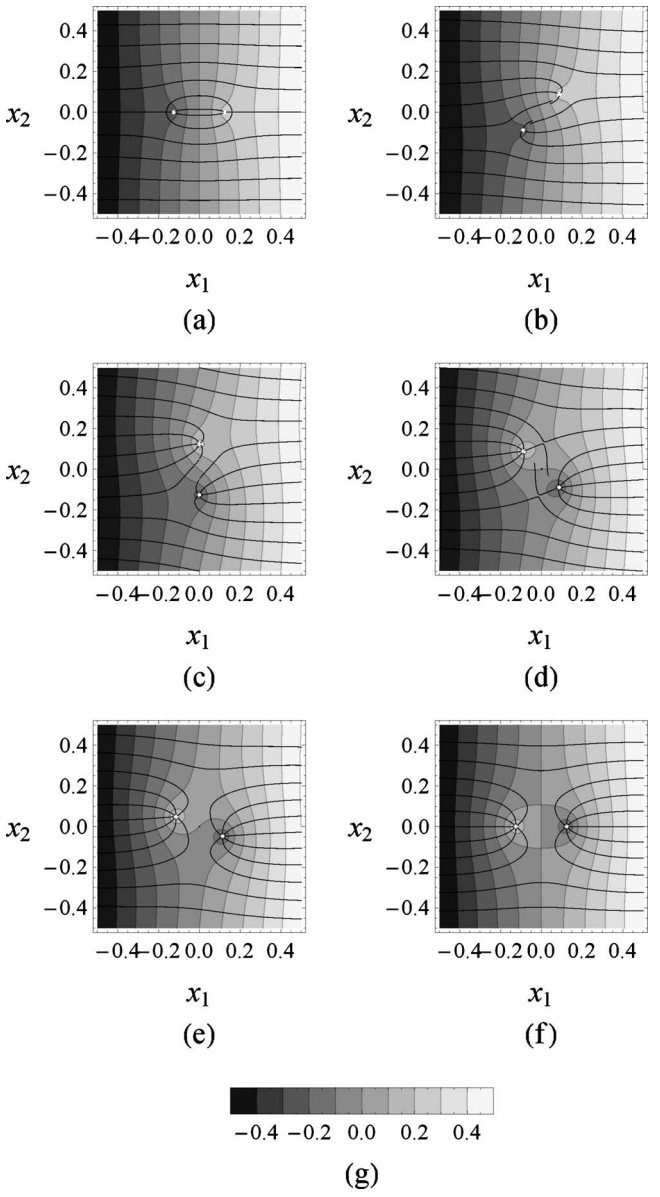

FIG. 3. The pressure (4.8) in the unit two-dimensional square cell for various locations of the vertices a_1 and a_2. The distance between the vertices is equal to 0.125 and $a_1=-a_2=a/2$, where a_1 is the angle in radians with the x_1 axis. Data are for (a) $a_1=0$, (b) $\frac{\pi}{4}$, (c) $\frac{\pi}{2}$, (d) $\frac{3\pi}{4}$, (e) $\frac{7\pi}{8}$, and (f) π. The velocity vector field $\mathbf{v}=-K\nabla p$ is shown by streamlines ($K=1$). Gray levels are given in (g). The small regions in all the subfigures out of the range $[-0.5,0.5]$ (near the vertices) are displayed in white.

$$j=J_2-J_1. \tag{4.4}$$

One of the relations (3.23) is deduced from the equality $p_{1'}=p_1-1$ and Eq. (4.2),

$$P_2=1-P_1. \tag{4.5}$$

Formula (3.27) takes the form (see also the two-dimensional example VIIB from [3])

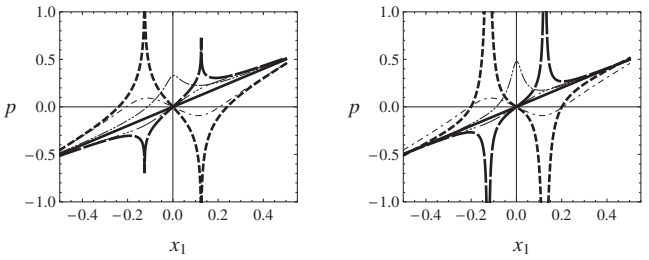

FIG. 4. The pressure as a function of x_1 on two intervals $-0.5 < x_1 < 0.5$ with $x_2=0$ and $x_2=0.1$ for the three locations of $\mathbf{a}_1$ and $\mathbf{a}_2$ shown in Fig. 2. (a) 2D case; (b) three-dimensional case. Data are for $\mathbf{a}=(0.25,0,0)$: bold –, $x_2=0$; $-\cdots-$, $x_2=0.1$; $\mathbf{a}=(0,0.25,0)$: bold –, $x_2=0$; $-\cdots-$, $x_2=0.1$; $\mathbf{a}=(-0.25,0,0)$: bold –, $x_2=0$; $-\cdot-$, $x_2=0.1$.

$$P_1 = \frac{j}{2}\left(\frac{2}{\pi}\ln\frac{|\sigma(a)|}{r} - |a|^2\right) + \mathrm{Re}\, a, \tag{4.6}$$

where the overbar stands for the complex conjugation and Re stands for the real part. Therefore, the system with respect to J_1, J_2, P_1, P_2, and j consists of the five equations (4.2)–(4.6) which can be easily solved; j is derived as

$$j = \frac{\alpha_2 - (\alpha_1+\alpha_2)\mathrm{Re}\, a}{1 + \frac{1}{2}(\alpha_1+\alpha_2)\left(\frac{2}{\pi}\ln\frac{|\sigma(a)|}{r} - |a|^2\right)}, \tag{4.7}$$

from which the other quantities follow. The local pressure is given by

$$p(z) = -\frac{j}{2\pi}\ln\frac{|\sigma(z-a/2)|}{|\sigma(z+a/2)|} + \mathrm{Re}\left[\left(1 - \frac{\bar{a}}{2}j\right)z\right]. \tag{4.8}$$

In Fig. 3, the pressure $p(z)$ is displayed for various locations of the vertices, i.e., for various values of the complex number a; $\alpha=\alpha_1=\alpha_2$ and r are equal to 1 and 0.05, respectively. Since the external pressure gradient is equal to (1,0), pressure is an increasing function of x_1 when the field is not too disturbed by the resurgences as it can be seen in Fig. 3(a), for instance, where $a=0.25$. Then, the two vertices are rotated while keeping a constant distance between them. As soon as the angle θ is larger than $\pi/2$, p is not anymore a monotonous function of x_1 and it displays some interesting features [see Figs. 3(c)–3(e)]. When $\theta=\frac{\pi}{2}$, two isolated "islands" of high and low pressures are created with a large zone where the velocities are inverted.

In Fig. 4(a), the pressure $p(z)=p(x_1,x_2)$ is shown as a function of x_1 with fixed $x_2=0$ and $x_2=0.1$ for three locations of the centers $\mathbf{a}_1$ and $\mathbf{a}_2$. For $a=\pm 0.25$, pressure presents logarithmic singularities at $x_1=\pm 0.125$ which belong to the interval $-0.5<x_1<0.5$; note that the four peaks shown in Fig. 4(a) go to infinity, but they are truncated by the drawing software. The amplitudes of the peaks show that the value of $p(x_1,0)$ for $x_1=\pm 0.125$ in the case $a=-0.25$ tends to infinity faster than in the case $a=0.25$. For $a=0.25i$ (i denotes the imaginary unit $\sqrt{-1}$), the pressure $p(x_1,0)$ is almost a linear function of x_1.

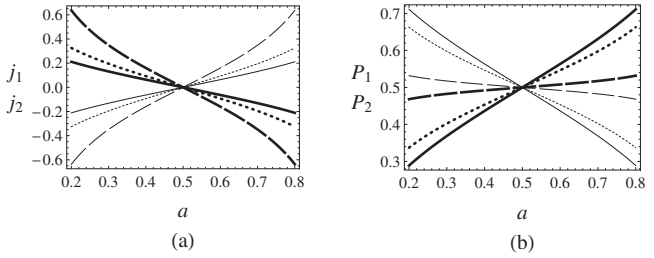

FIG. 5. Two-dimensional medium. (a) The flow rates $j_1=j$ and $j_2=-j$ as functions of a calocated by Eq. (4.7) for different α when a is real [see Fig. 2(a)]; j_1 (thick lines) and j_2 (thin lines). (b) The pressure differences P_1 and P_2 calculated by Eqs. (4.5) and (4.6); conventions are the same as in (a); P_1 (thick lines) and P_2 (thin lines). Data are for $\alpha=0.5$ (solid line), $\alpha=1$ (dotted line), and $\alpha=10$ (dashed line).

In the same figure, the pressure $p(x_1,0.1)$ is shown in the interval $-0.5<x_1<0.5$ which does not contain the singular points. The perturbations from the linear variations with x_1 are greater for $a=-0.25$ than for $a=0.25$. For $a=0.25i$, backflow is observed near the point (0,0.1).

The flow rates j_n and the pressure differences P_n ($n=1,2$) are displayed in Fig. 5 for $\alpha=1$ and $0.2<a<0.8$, where $j_1=j$ and $j_2=-j$ are calculated by Eq. (4.7), and P_n by Eqs. (4.5) and (4.6). When the centers of the injection domains are periodically arranged along the x_1 axis ($a=0.5$), the flow rates vanish and $P_1=P_2=0.5$. When a is replaced with $1-a$, the following symmetry relations have to be fulfilled: $j_2(a)=j_1(1-a)$ and $P_2(a)=1-P_1(1-a)$. These relations can be considered as a precision criterion of approximations (4.5)–(4.7). Although these relations do not verify the symmetry relations analytically, Fig. 5 shows that the corresponding numerical results verify symmetry quite closely.

Permeability is calculated by Eq. (3.44). Consider for definiteness the (1,1) component of $\bar{\mathbf{K}}_1$,

$$K_{11} = 1 - (a_{11}j_1 + a_{21}j_2) - (J_1R_{11} + J_2R_{21}), \tag{4.9}$$

where $\mathbf{R}_1=(R_{11},R_{12})$ and $\mathbf{R}_2=(R_{21},R_{22})$. The vector $\mathbf{R}_1$ connects the vertices $\mathbf{a}_1$ and $\mathbf{a}_2$, and $\mathbf{R}_2$ connects the vertices $\mathbf{a}_{2'}=\mathbf{a}_2+(1,0)$ and $\mathbf{a}_1$ (see Fig. 2). Hence, $\mathbf{R}_1=-(\mathrm{Re}\, a,\mathrm{Im}\, a)$ and $\mathbf{R}_2=-(\mathrm{Re}[1-a],\mathrm{Im}[1-a])$. Substitution of these values and of Eqs. (4.6) and (4.7) into Eq. (4.9) and the use of Eqs. (4.2)–(4.5) yield

$$K_{11} = 1 + \frac{2\alpha_1(\mathrm{Re}\, a)^2 + \alpha_2[1 - 3\ \mathrm{Re}\, a + 2(\mathrm{Re}\, a)^2]}{1 + \frac{\alpha_1+\alpha_2}{2}\left(\frac{2}{\pi}\ln\frac{|\sigma(a)|}{r} - |a|^2\right)}. \tag{4.10}$$

For $\alpha=\alpha_1=\alpha_2$, Eq. (4.10) becomes

$$K_{11} = 1 + \alpha\frac{1 - 3\ \mathrm{Re}\, a + 4\ \mathrm{Re}\, a^2}{1 + \alpha\left(\frac{2}{\pi}\ln\frac{|\sigma(a)|}{r} - |a|^2\right)}. \tag{4.11}$$

For large α, one can see that whatever the value of the complex number a the permeability K_{11} tends toward a linear function of α,

$$K_{11} = 1 + \frac{\alpha}{2}. \tag{4.12}$$

Moreover, it is worth noting that formulas (4.11) and (4.10) hold for $|a| \leq 0.5$. One cannot formally replace a with $1-a$, since the pressure difference P_1 in Eq. (4.6) has to be corrected by the jump 0.5 [see also Fig. 5(b)].

Figure 6(a) displays K_{11} as a function of α for various real values of a and $r=0.1$; of course, K_{11} is an increasing function of α. Figure 6(b) also displays K_{11} as a function of α, but for the three configurations in Fig. 2, including the complex value of a; K_{11} increases with the length of the network edges.

Figure 6(c) displays K_{11} as a function of a when it is real for various values of α_1 and α_2 with fixed $r=0.05$. Only for α_1 much larger than α_2 permeability is an increasing function of a. Such a behavior is similar to the classic case of the parallel networks with independently conducting edges.

However, the most striking feature in Fig. 6(c) is the existence of a minimum in a. A simple model can be devised in order to derive it. View the physical situation as a first resistance α_1^{-1} in parallel with a length a of porous medium of resistance $a/K=a$; this first set is in series with a resistance α_2^{-1} in parallel with a length $1-a$ of porous medium of resistance $1-a$. It is an elementary calculation to derive the equivalent approximate conductivity K_{app} of these two sets,

$$K_{app} = \left(\frac{a}{1 + a\alpha_1} + \frac{1-a}{1 + (1-a)\alpha_2} \right)^{-1}. \tag{4.13}$$

Note that this trivial formula yields correct orders of magnitude. Moreover, this function has always an extremum for

$$a = \frac{\alpha_2}{\alpha_1 + \alpha_2}. \tag{4.14}$$

This elementary prediction is in acceptable agreement with the full results. It also predicts the fact that a is a decreasing function of the ratio α_1/α_2.

A slightly more refined model can be derived when the resistance of the continuum is approximated by the resistance between two nonoverlapping disks of radius r with a distance between the centers equal to d,

$$\mathcal{R}(d) = \frac{1}{\pi} \ln \frac{1 + \frac{2r}{d} + \sqrt{1 - \left(\frac{2r}{d}\right)^2}}{1 + \frac{2r}{d} - \sqrt{1 - \left(\frac{2r}{d}\right)^2}}. \tag{4.15}$$

Then, the equivalent approximate conductivity K_{app} becomes

$$K_{app} = \left(\frac{1}{\mathcal{R}(a)^{-1} + \alpha_1} + \frac{1}{\mathcal{R}(1-a)^{-1} + \alpha_2} \right)^{-1}. \tag{4.16}$$

The calculations with formulas (4.10), (4.13), and (4.16) are compared in Fig. 6(d). The three functions have minima for $a < 0.5$ equal to 0.2788, 0.375, and 0.4708, respectively, for various α_1 and α_2. For $\alpha_1 = \alpha_2$, only permeability (4.11) has such a minimum.

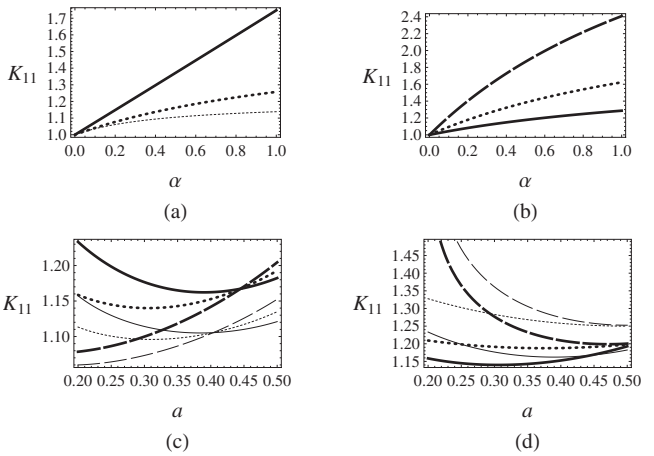

FIG. 6. The permeability K_{11} in two and three dimensions as a function of [(a) and (b)] α and [(c) and (d)] a (a real). (a) K_{11} in two [Eq. (4.11), thick lines] and three [Eq. (4.25), thin lines] dimensions, respectively, for the vertices depicted in Fig. 2(a); data are for $a=0.1$ (solid line) and 0.4 (dotted line). (b) K_{11} in two dimensions [Eq. (4.11)] for different locations of $\mathbf{a}_1$ and $\mathbf{a}_2$; data are for $a=0.3$ (solid line), $a=0.3i$ (dotted line), and $a=-0.3$ (dashed line). (c) K_{11} in two dimensions calculated with Eq. (4.10) (thick lines) and in three dimensions with Eq. (4.24) (thin lines) for $\mathbf{a}=(a,0,0)$; data are for $\alpha_1=\alpha_2=0.5$ (solid line), $\alpha_1=0.5$ and $\alpha_2=0.3$ (dotted line), and $\alpha_1=0.5$ and $\alpha_2=0.1$ (dashed line). (d) K_{11} in two dimensions; data are for $\alpha_1=0.5$, $\alpha_2=0.3$, $r=0.1$ (thick lines) and for $\alpha_1=\alpha_2=0.5$, $r=0.1$ (thin lines) calculated with Eq. (4.10) (solid line), Eq. (4.13) (dotted line), Eq. (4.16) (dashed line).

B. Three-dimensional example

The same example as in Sec. IV A is now addressed in three dimensions; the third coordinate to be added in Eq. (4.1) is always equal to zero. Consider a periodic structure represented by the unit cubic cell ($\ell_1=\ell_2=\ell_3=1$) with two vertices $\mathbf{a}_1=(a_{11},a_{12},a_{13})$ and $\mathbf{a}_2=(a_{21},a_{22},a_{23})$ sequentially connected as shown in Fig. 2. An external pressure gradient $\overline{\nabla p}=(1,0,0)$ is applied. Equations (4.3) and (4.4) hold. According to Eq. (3.20),

$$p_1 = \frac{j}{4\pi r} - \frac{j}{4\pi}\wp(\mathbf{a}) + \mathbf{b}\cdot\mathbf{a}_1 + p_0, \tag{4.17a}$$

$$p_2 = -\frac{j}{4\pi r} + \frac{j}{4\pi}\wp(\mathbf{a}) + \mathbf{b}\cdot\mathbf{a}_2 + p_0, \tag{4.17b}$$

where $\mathbf{a}=\mathbf{a}_1-\mathbf{a}_2=(a_1,a_2,a_3)$; p_0 is an arbitrary constant which can be equated to zero.

Then, Eq. (3.27) takes the form

$$P_1 = -\frac{j}{2\pi}\left[-\frac{1}{r} + \wp(\mathbf{a}) + \frac{1}{2}\sum_{k,l=1,2,3} \gamma_{lk} a_l a_k \right] + a_1. \tag{4.18}$$

Introduction of expression (3.10) for a cubic cell into Eq. (4.18) yields

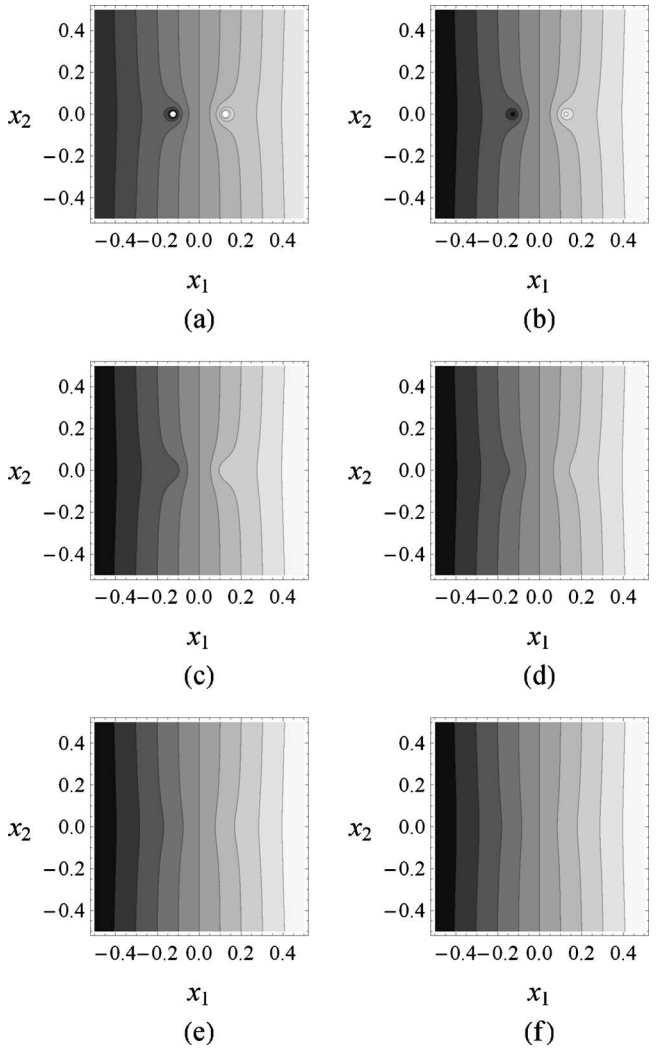

FIG. 7. Three-dimensional pressure field calculated with Eq. (4.23) for configuration of Fig. 2(a): $\mathbf{a}_1=(0.125,0,0)$ and $\mathbf{a}_2=(-0.125,0,0)$ in different sections of the unit cube. For all sections $-0.5<x_1<0.5$, $-0.5<x_2<0.5$; the third coordinate is fixed in each section: (a) $x_3=0$, (b) $x_3=0.02$, (c) $x_3=0.04$, (d) $x_3=0.08$, (e) $x_3=0.12$, and (f) $x_3=0.16$. Gray levels are the same as in Fig. 3(g).

$$P_1 = -\frac{j}{2\pi}\left[-\frac{1}{r}+\wp(\Delta\mathbf{a})\right]+\mathbf{b}\cdot\mathbf{a}. \tag{4.19}$$

Calculate $\mathbf{b}$ by Eq. (3.18),

$$\mathbf{b} = \mathbf{i}_1 - \frac{j}{3}\mathbf{a}. \tag{4.20}$$

Then, Eq. (4.19) becomes

$$P_1 = -\frac{j}{2\pi}\left[-\frac{1}{r}+\wp(\mathbf{a})+\frac{2\pi}{3}|\mathbf{a}|^2\right]+a_1. \tag{4.21}$$

Therefore, the system with respect to J_1, J_2, P_1, P_2, and j consists of the five equations (4.2)–(4.5) and (4.21). j is derived as in the previous example,

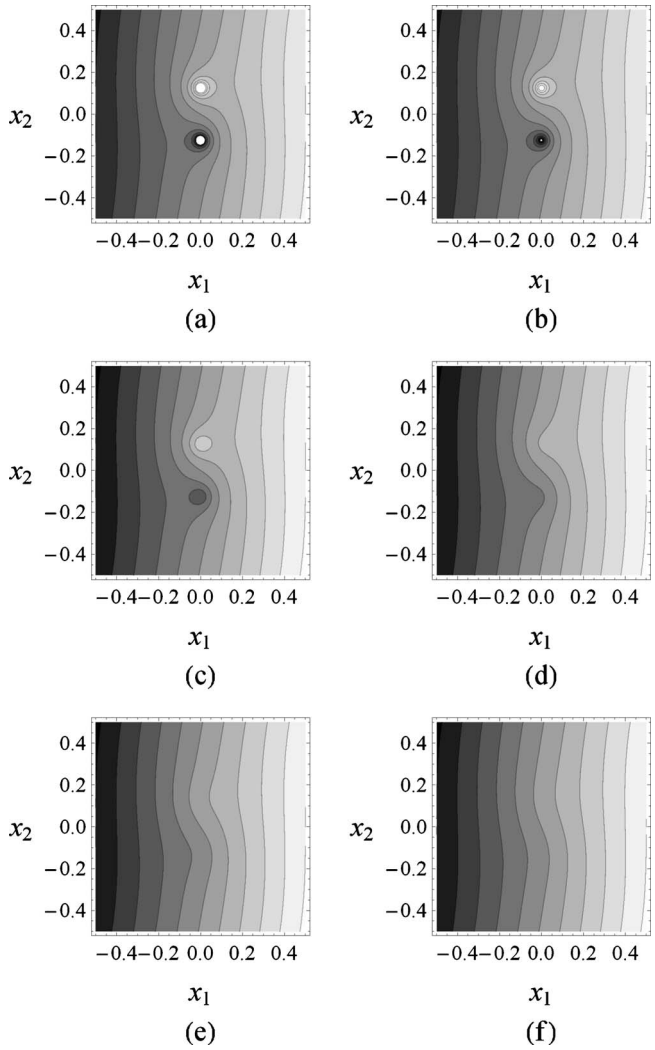

FIG. 8. Three-dimensional pressure field calculated with Eq. (4.23) for configuration of Fig. 2(b): $\mathbf{a}_1=(0,0.125,0)$ and $\mathbf{a}_2=(0,-0.125,0)$. Conventions are the same as in Fig. 7.

$$j = \frac{\alpha_2-(\alpha_1+\alpha_2)a_1}{1+\frac{1}{2\pi}(\alpha_1+\alpha_2)\left[\frac{1}{r}-\wp(\mathbf{a})-\frac{2\pi}{3}|\mathbf{a}|^2\right]}. \tag{4.22}$$

The local pressure Eq. (3.14) becomes

$$p(\mathbf{x}) = \frac{j}{4\pi}\left[\wp(\mathbf{x}-\mathbf{a}/2)-\wp(\mathbf{x}+\mathbf{a}/2)-\frac{1}{3}\mathbf{a}\cdot\mathbf{x}\right]+x_1. \tag{4.23}$$

In Figs. 4(b) and 7–9, the pressure $p(\mathbf{x})$ is presented for the three spatial locations of the vertices shown in Fig. 2 in accordance with Eqs. (4.1). In all cases, the external pressure gradient is directed along the x_1 axis, $\alpha=\alpha_1=\alpha_2=1$, and $r=0.05$. These three cases correspond to Figs. 3(a), 3(c), and 3(f) in two dimensions.

The corresponding pressure fields in three dimensions are displayed in Figs. 7–9. The fields are given for various values of x_3. Of course, $x_3=0$ corresponds to the plane where

the two vertices are present. These fields present some interesting features that we shall now summarize.

Let us start with the simplest case $\mathbf{a}_1=-\mathbf{a}_2=(0.125,0,0)$. The pressure field displayed in Fig. 7(a) for $x_3=0$ is qualitatively very similar to the 2D case displayed in Fig. 3(a). When $x_3\neq 0$, pressure becomes more uniform and the influence of the two vertices is a decreasing function of $|x_3|$ in agreement with what was already observed in two dimensions.

The second case where the axis of the vertices is perpendicular to the pressure is displayed with the same conventions in Fig. 8. In the plane $x_3=0$, the pressure field is much more disturbed than in the 2D case [see Fig. 3(c)]. The flow is very disturbed and locally inverted. The influence of x_3 is the same for obvious reasons.

Finally, the third case with antisymmetric vertices displayed in Fig. 9 is very close in nature to the 2D case [see Fig. 3(f)]. For instance, the recirculation zones are of about the same size and shape.

The pressure evolution along the x_1 axis is given in Fig. 4(b) for an easy comparison with the two-dimensional case. This figure presents the pressure on the interval $-0.5<x_1<0.5$ with $x_2=0$ and on the interval parallel to the x_1 axis determined by $-0.5<x_1<0.5$ and $x_2=0.1$. In the three-dimensional case, the interval belongs to the plane $x_3=0$. The three different locations of the points $(\mathbf{a}_1,\mathbf{a}_2)$ shown in Fig. 2 are considered. Of course, pressure has singularities at $(\pm 0.125,0,0)$. The peaks show that pressure in the three-dimensional case with power singularity r^{-1} tends to infinity faster than pressure in the two-dimensional case with logarithmic singularity $\ln r$. An analogous dependence is observed when the singular points are located at $(0,\pm 0.125,0)$; then, the pressure disturbance at (0,0,0) is higher than at (0,0) in the two-dimensional case. Therefore, as expected, the power singularity impacts more significantly on its neighborhood than the logarithmic singularity. When the singular points are located at $(0,\pm 0.125,0)$, pressure is almost a linear function of x_1 as in two dimensions.

In Fig. 4(b), $p(x_1,0.1,0)$ is also displayed for $-0.5<x_1<0.5$; along this interval, the distance to the singular points is larger than 0.1. The perturbations of the linear function for $a=-0.25$ are larger than for $a=0.25$. For $a=0.25i$, backflow is observed near (0,0.1).

It is necessary to note that the numerical results in the first example are more precise than in the second one, since we use the classical Weierstrass functions in the two-dimensional case which are implemented to computer with high precision. Computation of the triply periodic functions is a difficult computational problem. Here, we use formula (3.11) up to the sixth order. A detailed numerical investigation reads unrealistic pressure oscillations near the vertices $\mathbf{a}_1$ and $\mathbf{a}_2$. For instance, the white left disk at Fig. 7(a) should be replaced with a black domain. Figure 7(c) is likely to contain small disks as Fig. 7(b), but with smaller radii. The numerical results for points sufficiently away from the injection domains appear to be correct as it is supported by computations in the two-dimensional case.

Permeability is calculated by formula (4.9) which is also valid in this three-dimensional case. Substitution of Eqs. (4.21) and (4.22) yields

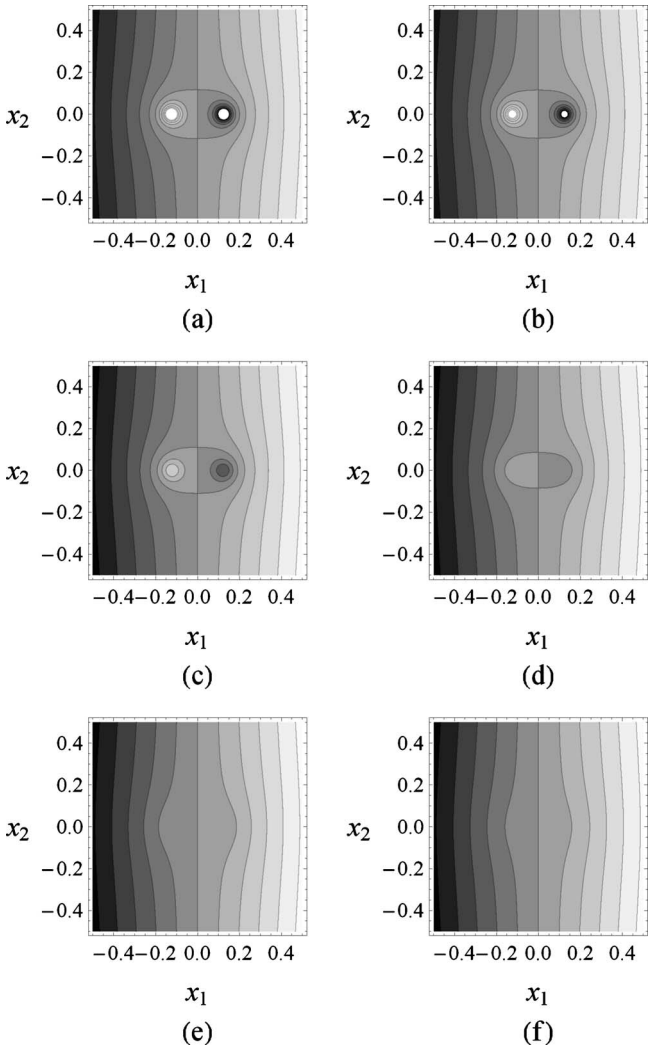

FIG. 9. Three-dimensional pressure field calculated with Eq. (4.23) for configuration of Fig. 2(c): $\mathbf{a}_1=(-0.125,0,0)$ and $\mathbf{a}_2=(0.125,0,0)$. Conventions are the same as in Fig. 7.

$$K_{11}=1+\frac{2\alpha_1 a_1^2+\alpha_2(1-3a_1+2a_1^2)}{1+\dfrac{\alpha_1+\alpha_2}{2\pi}\left(\dfrac{1}{r}-\wp(\mathbf{a})-\dfrac{2\pi}{3}|\mathbf{a}|^2\right)}. \quad (4.24)$$

For $\alpha=\alpha_1=\alpha_2$, Eq. (4.24) becomes

$$K_{11}=1+\alpha\frac{1-3a_1+4a_1^2}{1+\dfrac{\alpha}{\pi}\left(\dfrac{1}{r}-\wp(\mathbf{a})-\dfrac{2\pi}{3}|\mathbf{a}|^2\right)}. \quad (4.25)$$

Typical variations are shown in Figs. 6(a) and 6(c) where the permeabilities in two- and three-dimensional cases are compared. The three-dimensional permeability is greater than the two-dimensional one for sufficiently large a [compare the two solid lines in Fig. 6(c)]. Finally, K_{11} has also a minimum which can be explained as before by Eqs. (4.13)–(4.16).

C. Backflow in two and three dimensions

It follows from Sec. II of [3] that in one-dimensional media punctual resurgences never produce backflow in contrast

with extended resurgences. The present results and [3] imply that in two and three dimensions a backflow can occur for punctual resurgences as observed in the examples of Secs. IV A and IV B.

The first example concerns a two-dimensional flow in a doubly periodic medium represented by the unit square. The vertices of the graph $\mathbf{a}_1$ and $\mathbf{a}_2$ are located on the opposite points of the circle of the radius 0.25 centered at the origin. First, $\mathbf{a}_1$ and $\mathbf{a}_2$ lie on the x_1 axis as shown in Fig. 2(a). One can observe a small disturbance of the uniform flow in Fig. 3(a). $v_1(x_1,x_2)$ at each point out of the injection domains has the same sign as $-\boldsymbol{\nabla} p$. Then, the "dipole" $\mathbf{a}_1,\mathbf{a}_2$ turns and makes an angle from 0° to 180° with the direction of the external flow, i.e., with the x_1 axis as shown in Fig. 2. Despite an identical topology, its location in the continuous medium drastically influences flow. Domains of high and low pressures arise near the vertices $\mathbf{a}_1$ and $\mathbf{a}_2$, respectively, and they induce backflow as demonstrated in Figs. 3(c)–3(f). The total permeability coefficient K_{11} has the form (4.10). If the network is embedded in the bulk medium as shown in Fig. 2(a), K_{11} increases with α as shown in Fig. 6(a).

The second example concerns the flow in the three dimensions for which flow has a more complicated structure than in two dimensions. The pressure along the segment $-0.5 < x_1 < 0.5$, $x_2=0.1$ of the plane $x_3=0$ is presented for various locations of the vertices $\mathbf{a}_1$ and $\mathbf{a}_2$ in Fig. 4. Figures 7–9 present the pressure distribution in sections parallel to the plane $x_3=0$. Backflow occurs in the plane $x_3=0$ where the vertices lie. Comparison of Figs. 3(c) and 8 demonstrates that the pressure level lines in two-dimensional case posses lower curvature than the level lines in three-dimensional case near the injection domains.

V. CONCLUSION

Solutions are given for flow in a three-dimensional porous medium with resurgences when the injection domains are small. General formulas are given such as Eq. (3.44) for permeability.

The examples which are worked out show that backflow is common in two and three dimensions with punctual resurgences. This phenomenon was shown in [3] to occur only for extended resurgences for one-dimensional flow.

The considered resurgence problem has interesting mathematical properties. As it was noted in [3], it is nonlocal, i.e., the potential p satisfying the continuum Laplace equation is related via the network at $\mathbf{x}$ with values of p far away from the point at $\mathbf{x}$. Resurgence flows create a novel class of problems to be considered on structures obtained by superposing Riemann manifolds of different dimensions. Such structures which are called stratified sets are described in the last chapter of [13] where Poincaré's inequality, the weak maximum principle, and the Dirichlet boundary value problem are discussed. These first results on stratified sets are obtained under some geometrical restrictions. However, it should be emphasized that the porous media with resurgences as defined and discussed in the present paper do not satisfy the restrictions of [13]. Therefore, general questions such as the existence and uniqueness of solutions are still open. The present paper is devoted to the derivation of constructive solutions to these problems. The analytical formulas for the pressure and for the macroscopic permeability are deduced in the dilute case, i.e., when the injection domains are located sufficiently far away one from another. It would be very interesting to extend these results to general stratified sets.

Extension to time-dependent problems was already noted in [3] to be very important; compressibility effects should be taken into account as in the well tests routinely performed in the oil industry. In such cases, capillaries may also work as capacities able to store fluid. Very different behaviors are likely to occur. Such an analysis could be extended to other phenomena such as dispersion which has already been studied in fractured media by means of the detailed approach of [14].

Another class of phenomena would be solid mechanics where as mentioned in the Introduction reticulated structures studied by [6,7] among others could interact with continuous solids. On one hand, the reticulated structures correspond to the network and, on the other hand, the solid medium could be described by the classical continuum theory.

[1] G. I. Barenblatt, I. P. Zheltov, and I. N. Kochina, J. Appl. Math. Mech. **24**, 1286 (1960).

[2] I. I. Bogdanov, V. V. Mourzenko, J.-F. Thovert, and P. M. Adler, Water Resour. Res. **39**, 1023 (2003).

[3] P. M. Adler and V. M. Mityushev, Phys. Rev. E **79**, 026310 (2009).

[4] M. Barthélémy and Luis A. Nunes Amaral, Phys. Rev. Lett. **82**, 3180 (1999).

[5] D. Gibert, F. Nicollin, B. Kergosien, P. Bossart, C. Nussbaum, A. Grislin-Mouëzy, F. Conil, and Nasser Hoteit, Appl. Clay Sci. **33**, 21 (2006).

[6] G. P. Panasenko, Int. J. Comput. Civil Struct. Eng. **1**, 57 (2000).

[7] D. Cioranescu and J. Saint Jean Paulin, *Homogenization of Reticulated Structure*, Applied Mathematical Sciences Vol. 136 (Springer Verlag, Berlin, 1999).

[8] V. L. Berdichevskij, *Variational Principles of Continuum* (Nauka, Moscow, 1983).

[9] P. M. Adler and H. Brenner, PCH, PhysicoChem. Hydrodyn. **5**, 245 (1984).

[10] P. M. Adler, *Porous Media: Geometry and Transport* (Butterworth-Heinemann, Stoneham, MA, 1992).

[11] R. Landauer, in *Electrical Conductivity in Inhomogeneous Media*, Electrical Transport and Optical Properties of Inhomogeneous Media, edited by J. C. Garland and D. B. Tanner (AIP, New York, 1978).

[12] N. I. Akhiezer, *Elements of the Theory of Elliptic Functions* (American Mathematical Society, Providence, RI, 1990).

[13] Yu. V. Pokornyi, O. P. Penkin, V. L. Pryadiev, A. V. Borovskikh, K. P. Lazarev, and S. A. Shabrov, *Differential Equations on Geometrical Graphs* (Fizmatlit, Moscow, 2004) (in Russian).

[14] O. Huseby, J.-F. Thovert, and P. M. Adler, Phys. Fluids **13**, 594 (2001).